J Eng Math (2008) 61:1–16
DOI 10.1007/s10665-007-9155-5

Dynamics of advanced rotating blades made of functionally graded materials and operating in a high-temperature field

Liviu Librescu · Sang-Yong Oh · Ohseop Song · Ho-Sik Kang

Received: 13 November 2006 / Accepted: 8 May 2007 / Published online: 26 July 2007

Abstract Problems involving the modeling and free vibration of pre-twisted rotating blades made of functionally graded materials (FGMs) and operating in a high-temperature field are considered. The blade, mounted on a rigid hub, is modeled as a thin-walled beam that incorporates the warping restraint and the pre-twist effects. As a result of the latter feature, an extension-twist elastic coupling is induced. Consistent with the concept of the FGM structures, the two constituent materials, ceramic and metal, experience a continuous variation across the beam wall thickness, and, as a result, the adverse effects featured by the standard laminated structures, such as delamination/debonding, are precluded to occur. Numerical results highlighting the effects of the extension-twist elastic coupling considered in conjunction with the volume fraction of the two constituent phases and of the thermal degradation of material properties on eigenfrequencies are presented, and pertinent conclusions are outlined. Comparisons of predictions, as well as validations of results against those obtained in some special cases, which are available in the specialized literature, are also supplied. In addition to a better understanding of the implication of incorporation of FGMs, the results of this research can be instrumental toward the reliable design of advanced turbomachinery blades that operate in a high-temperature environment.

Keywords Free vibration · Functionally graded materials · Rotating blades · Thermal degradation · Twist-extension coupling

1 Introduction

It is a well-known fact that, during their operational life, gas-turbine blades are exposed to severe environments consisting, among others, of time-dependent high-temperature fields and thermal shocks. Due to induced vibration,

Professor Liviu Librescu died a heroic death on April 16, 2007, while protecting the lives of his students in a Virginia Tech classroom. This paper was virtually accepted for publication with laudatory reviews two weeks before his death.

L. Librescu
Department of Engineering Science and Mechanics, Virginia Polytechnic Institute and State University, Blacksburg, VA, USA

S.-Y. Oh · O. Song (✉) · H.-S. Kang
Department of Mechanical Engineering, Chungnam National University, Daejeon 305-764, South Korea
e-mail: songos@cnu.ac.kr

catastrophic, or in the best-case scenario, fatigue failures of blades can occur. Moreover, in order to enhance their efficiency, increases of the operating temperature field are needed.

A similar situation is valid with the flexible space booms attached to spinning satellites which, due to the rapid temperature changes at day-night transitions in orbit, are exposed to a catastrophic dynamic instability referred to as the *thermal flutter*. In order to preclude such damaging phenomena from occurring, to increase their efficiency and ensure long-life structurally sound turbomachinery blades, two basic issues have to be properly addressed:

1. Incorporation of advanced-material systems capable of withstanding high-temperature fields and thermal shocks. Among the best candidates that can address this requirement are functionally graded materials (FGMs).
   As is well known, these materials, developed for high-temperature structural applications are composed of different constituents, such as ceramics and metals, with a continuously graded variation in composition across their wall thickness.
   Metal–ceramic FGMs combine synergistically the positive properties of these two constituents, in the sense that the ceramic in a FGM offers thermal-barrier capabilities and protects the metal from corrosion and oxidation, while the FGM is toughened and strengthened by the metallic composition. As a result, these materials are able to withstand high-temperature gradients, without structural failure.
   Moreover, in contrast to standard laminated composite structures whose material properties are piecewise constant through the wall thickness, and, as a result, are exposed to adverse interface effects that can yield the failure of the structure, in the case of the FGMs, due to the smooth variation of their material properties, the occurrence of such effects is precluded.
   In addition to the research work devoted to modeling of 3-D FGM media, the studies involving thin-walled structures made up of FGMs have been mainly devoted to beams, plates and shells. To the best of the authors' knowledge, in spite of its evident practical importance and of the work done on vibration of FGM structures, (see the review paper [1]), with the exception of the results in [2,3] and of those contained in a recently appeared monograph by Librescu and Song [4], no research work related to the modeling and behavior of rotating blades featuring the elastic twist–extension coupling, operating in a high-temperature environment and made of FGMs has been accomplished yet.
2. The second problem considered in conjunction with the former, should consist of a thorough analysis of their vibrational behavior.
   Such a study should provide a better understanding of the implications of the incorporation of such advanced-material systems, and, implicitly, should help their reliable design.
   Herein, the case of a straight, pre-twisted thin-walled beam of variable cross-section, rotating with a constant angular speed and exposed to a steady-state temperature field experiencing a gradient through the blade thickness is considered. It is assumed that the blade is made of FGMs whose properties vary continuously across the blade thickness and that the material properties are temperature-dependent. In this context, both the modeling and the vibrational behavior of rotating blades are investigated, and pertinent conclusions are outlined.
   While representing an extension of the research done in [5], in the sense of its generalization by including the concept of FGM in conjunction with the existence of a thermal field, the results supplied here highlight the great performances obtained when, in the context of this structural systems, FGMs are incorporated.

2 Structural model

2.1 Basic assumptions

It is considered that the blade, of non-uniform cross-section and of length L, is mounted on a rigid hub of radius R_0 and is rotating with the constant angular velocity $\mathbf{\Omega}(= \Omega\mathbf{j} = \Omega\mathbf{J})$. The origin of the *rotating* axis system (x, y, z)

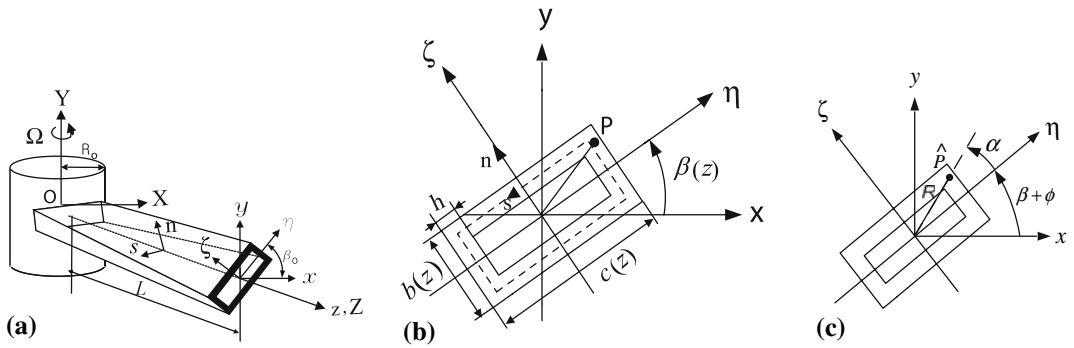

Fig. 1 (**a**) Configuration of the pretwisted rotating thin-walled beam, (**b**) Box-beam cross-section before deformation, (**c**) Box-beam cross-section after deformation

with the associated unit vectors $(\mathbf{i}, \mathbf{j}, \mathbf{k})$ is fixed at the blade root at an offset R_0 from the rotation axis (Fig. 1a), where z is the spanwise coordinate, x and y being the cross-sectional coordinates.

In addition, three other coordinate systems are adopted: one of these, the inertial one, (X, Y, Z), with the unit vectors (I, J, K) is considered to be attached to the center of the hub O (see Fig. 1a), the y- and Y-axes being parallel at any time t, while the other one is the curvilinear (η, ζ, z) system shown in Fig. 1b, c. The axes η and ζ are the principal axes of the beam cross-section located in the cross-sectional planes of the beam, with the origin coinciding with that of the axis Z. Axes η and ζ are orthogonal and rotate about the z-axis with the cross-section due to the built-in twist.

Finally, a local system of orthogonal Cartesian coordinates (s, z, n) is also considered, where s and n are the circumferential and the thicknesswise coordinates, respectively, (see Fig. 1).

It should be stressed that, due to the assumed non-uniformity of the beam in the spanwise direction, x and y become functions of both the circumferential and spanwise coordinates, s and z, respectively, implying that $x \equiv x(s, z)$ and $y \equiv y(s, z)$.

One should indicate here that two approaches involving the modeling of rotating pre-twisted blades are in use. One of these, attributed to Wagner, is based on the widely accepted helical multifilament concept, used, among others, by Houbolt and Brooks [6], Kaza and Kielb [7] and McGee [8]. Within the other one, the tensorial approach enabling one to convert the quantities evaluated in the curvilinear (η, ζ, z) system to the local Cartesian one (s, z, n) was prompted by Washizu [9] and applied by Bauchau and Hong [10].

In the paper by Oh et al. [5] and the monograph by Librescu and Song [4], both methods have been illustrated, and excellent agreements of predictions have been reached. Within the forthcoming developments, the methodology by Wagner will be only applied. Throughout this paper it is assumed that: (i) the original cross-section of the beam is preserved, implying that the projection of the cross-section on the plane normal to the z-axis does not distort during deformation, (ii) the concept of the Saint-Venant torsional model is discarded in favor of the non-uniform torsional one, (iii) in addition to the primary warping, the secondary warping effect associated with points off the mid-line contour, is also incorporated, and (iv) the effects of presetting and precone angles are not included in the present modeling.

In order to render the paper reasonably self-contained, a few preliminary kinematical results will be supplied next.

2.2 Kinematics

The position vector of an arbitrary point belonging to the deformed beam structure is expressed as:

$$\mathbf{R} = (x + u)\,\mathbf{i} + (y + v)\,\mathbf{j} + (z + R_0 + w)\mathbf{k}, \tag{1}$$

where u, v and w are the displacements in the directions x, y and z, respectively. Recalling that the spin rate is constant, keeping in mind that the rotation takes place solely in the XZ-plane, and making use of equations

expressing the time derivatives of unit vectors (**i, j, k**), one obtains the velocity and acceleration vectors of an arbitrary point M of the pretwisted rotating beam as

$$\dot{\mathbf{R}} = V_x\mathbf{i} + V_y\mathbf{j} + V_z\mathbf{k}, \quad \ddot{\mathbf{R}} = a_x\mathbf{i} + a_y\mathbf{j} + a_z\mathbf{k}. \tag{2a, b}$$

Their components are as follows:

$$V_x = \dot{u} + (R_0 + z + w)\Omega, \quad V_y = \dot{v}, \quad V_z = \dot{w} - (x + u)\Omega, \tag{3a, b, c}$$

and

$$a_x = \ddot{u} + \underline{2\dot{w}\Omega} - \underline{\underline{(x + u)\Omega^2}}, \quad a_y = \ddot{v}, \quad a_z = \ddot{w} - \underline{2\dot{u}\Omega} - \underline{\underline{(R_0 + z + w)\Omega^2}}. \tag{4a, b, c}$$

In these and the following equations the superposed dots denote time derivatives, the primes denote differentiation with respect to the longitudinal z-coordinate, and the terms underscored by one or two superposed solid lines are associated with Coriolis and centrifugal inertias, respectively.

Paralleling the approach of [4], some preliminary results needed in the subsequent developments will be derived. To this end, we will consider the configuration of the pretwisted beam before and after deformation, (see Fig. 1b, c, respectively). Before deformation, the coordinates of a point P on the helical fiber of the beam cross-section expressed in terms of the distances η and ζ along the principal axes are

$$x(s, z) = \eta(s)\cos\beta(z) - \zeta(s)\sin\beta(z), \quad y(s, z) = \eta(s)\sin\beta(z) + \zeta(s)\cos\beta(z), \tag{5a, b}$$

while their rate of change with respect to z are

$$x' = -\beta' y; \quad y' = \beta' x, \tag{6}$$

where $\beta = \beta(z)$ denotes the pre-twist angle, while $\phi = \phi(z, t)$ the elastic twist angle.

Now, the position on the helical fiber after deformation of point $\hat{P}$ is provided by

$$\hat{x} = R\cos(\beta + \phi + \alpha) = \eta\cos(\beta + \phi) - \zeta\sin(\beta + \phi), \tag{7a}$$
$$\hat{y} = R\sin(\alpha + \beta + \phi) = \eta\sin(\beta + \phi) + \zeta\cos(\beta + \phi), \tag{7b}$$
$$\hat{z} = z + R_0 + w = z + R_0 + w_0(z, t) - \left[\overline{F} - nr_t\right]\phi', \tag{7c}$$

while their rate of change with respect to z is

$$\hat{x}' = -(\beta' + \phi')[\eta\sin(\beta + \phi) + \zeta\cos(\beta + \phi)], \tag{8a}$$
$$\hat{y}' = (\beta' + \phi')[\eta\cos(\beta + \phi) - \zeta\sin(\beta + \phi)], \tag{8b}$$
$$\hat{z}' = 1 + w_0' - [\overline{F} - nr_t]\phi'', \tag{8c}$$

where $w_0 = w_0(z, t)$ denotes the spanwise beam displacement.

In order to obtain the longitudinal strain in the helical fiber, expressions for $\mathrm{d}S/\mathrm{d}z$ and $\mathrm{d}s/\mathrm{d}z$ are needed. From (8) we get

$$(\mathrm{d}S/\mathrm{d}z)^2 = (\hat{x}')^2 + (\hat{y}')^2 + (\hat{z}')^2 = 1 + 2\{w_0' - (\overline{F} - nr_t)\phi''\} + (\beta' + \phi')^2(\eta^2 + \zeta^2), \tag{9}$$

and $(\mathrm{d}s/\mathrm{d}z)$, can be obtained directly from (9) by letting $\phi' = 0$, $\phi'' = 0$ and $w_0' = 0$.

Thus

$$(\mathrm{d}s/\mathrm{d}z)^2 = 1 + (\eta^2 + \zeta^2)(\beta')^2. \tag{10}$$

As a result, by adopting as valid the assumption by Houbolt and Brooks [6] according to which $(\eta^2+\zeta^2)(\beta')^2 << 1$, for the longitudinal strain ϵ_{zz} one obtains

$$\varepsilon_{zz} = (\mathrm{d}S - \mathrm{d}s)/\mathrm{d}s = w_0' - [\overline{F}(s, z) - nr_t(s, z)]\phi'' + \frac{1}{2}\left((\phi')^2 + 2\beta'\phi'\right)(\eta^2 + \zeta^2). \tag{11}$$

where $\overline{F}$ and r_t denote the primary and second warping functions, respectively. For their definition, see [4].

Using Eq. 11, one can cast ϵ_{zz} as

$$\varepsilon_{zz} = \varepsilon_{zz}^{(0)} + n\varepsilon_{zz}^{(1)}, \tag{12}$$

where

$$\varepsilon_{zz}^{(0)} = w_0' + \frac{1}{2}(\eta^2 + \zeta^2)[(\phi')^2 + 2\beta'\phi'] - \phi''\overline{F}, \quad \varepsilon_{zz}^{(1)} = r_t\phi''. \tag{13a,b}$$

For further use, a more elaborated expression of the acceleration components of the twisted rotating blade is needed. To this end, using the definitions

$$u(x, y, z; t) = \hat{x} - x = x(\cos\ \phi - 1) - y \sin\ \phi, \tag{14a}$$

$$v(x, y, z; t) = \hat{y} - y = x \sin\ \phi + y(\cos\ \phi - 1), \tag{14b}$$

$$w(x, y, z; t) = \hat{z} - (z + R_0) = w_0 - (\overline{F} - nr_t)\phi' \tag{14c}$$

in conjunction with (5) and (4) one obtains

$$a_x = -\ddot{\phi}(\eta N + \zeta M) - \dot{\phi}^2(\eta M - \zeta N) + \underline{2\Omega[\dot{w}_0 - \dot{\phi}'(\overline{F} - nr_t)]} - \underline{\underline{\Omega^2\ (\eta M - \zeta N)}}, \tag{15a}$$

$$a_y = -\ddot{\phi}(\zeta N - \eta M) - \dot{\phi}^2(\eta N + \zeta M), \tag{15b}$$

$$a_z = \ddot{w}_0 - \ddot{\phi}'(\overline{F} - nr_t) + \underline{2\Omega\dot{\phi}(\eta N + \zeta M)} - \underline{\underline{\Omega^2[R_0 + z + w_0 - \phi'(\overline{F} - nr_t)]}}, \tag{15c}$$

where, for brevity,

$$M \equiv \cos\ (\beta + \phi),\ N \equiv \sin\ (\beta + \phi). \tag{16}$$

3 3-D constitutive equations of functionally graded blades

Because the FGMs are isotropic, the corresponding thermoelastic constitutive law adapted to the case of thin-walled structures is expressed as

$$\begin{Bmatrix} \sigma_{ss} \\ \sigma_{zz} \\ \sigma_{zn} \\ \sigma_{ns} \\ \sigma_{sz} \end{Bmatrix} = \begin{bmatrix} Q_{11} & Q_{12} & 0 & 0 & 0 \\ Q_{12} & Q_{11} & 0 & 0 & 0 \\ 0 & 0 & Q_{44} & 0 & 0 \\ 0 & 0 & 0 & Q_{44} & 0 \\ 0 & 0 & 0 & 0 & Q_{66} \end{bmatrix} \begin{Bmatrix} \varepsilon_{ss} - \hat{\alpha}\Delta T \\ \varepsilon_{zz} - \hat{\alpha}\Delta T \\ \varepsilon_{zn} \\ \varepsilon_{ns} \\ \varepsilon_{sz} \end{Bmatrix}. \tag{17}$$

The reduced thermoelastic coefficients are defined as:

$$Q_{11} = \frac{E}{1 - \nu^2}, \quad Q_{12} = \frac{E\nu}{1 - \nu^2}, \quad Q_{66} = \frac{E}{2(1 + \nu)}\ (\equiv G), \quad Q_{44} = Q_{55} = k^2 G$$

$$\hat{\alpha} = \frac{E}{1 - \nu}\,\alpha, \tag{18a, b, c, d, e}$$

where E and ν are the Young's modulus and Poisson's ratio, respectively, k^2 is the transverse shear correction factor, ΔT is the steady-state temperature rise from that of the stress free state, while α is the thermal-expansion coefficient.

For the considered ceramic–metal FGM model, one postulates that the material properties vary continuously across the blade thickness according to the law

$$P(n) = E_c V_c(n) + E_m V_m(n), \tag{19}$$

where P denotes a generic thermoelastic material property. In an expanded form we have

$$E(n) = (E_c - E_m)V_c(n) + E_m, \quad \nu(n) = (\nu_c - \nu_m)V_c(n) + \nu_m, \tag{20a,b}$$

$$\rho(n) = (\rho_c - \rho_m)\ V_c(n) + \rho_m, \quad \alpha(n) = (\alpha_c - \alpha_m)\ V_c(n) + \alpha_m, \tag{20c,d}$$

where V_m and V_c are the volume fractions of metal and ceramic components fulfilling the relation $V_c(n)+V_m(n) = 1$, and subscripts m and c identify the quantities affiliated to metal and ceramic, respectively.

For the case of variation of constituents phases from ceramic to metal, V_c can be expressed as

$$V_c = [(2n + h)/2h]^K, \tag{21}$$

where h is the wall thickness of the blade, while K, $(0 \leq K \leq \infty)$, is the volume-fraction parameter, providing the material variation profile through the blade wall thickness. From (20), considered, in conjunction with (21), it results that for $n = h/2$, $V_c = 1$, this yielding $E \to E_c$, $\nu \to \nu_c$ and $\rho \to \rho_c$, whereas for $n = -h/2$, $V_c = 0$, where from $E \to E_m$, $\nu \to \nu_m$ and $\rho \to \rho_m$.

This shows that consistent with this law, the material properties vary continuously from the top surface of the blade where the material is entirely ceramic, to full metal at the bottom surface. From (21) it becomes evident that an increase of the volume-fraction parameter K from $K = 0$, for which the blade is entirely from ceramic, results in a continuous increase of the metal content in the detriment of the ceramic.

It is assumed that the blade is subjected to a steady-state thicknesswise temperature field, implying that $T = T(n)$.

The steady-state equation of the one-dimensional heat transfer is expressed by

$$\frac{\mathrm{d}}{\mathrm{d}n}\left[\kappa(n)\frac{\mathrm{d}T}{\mathrm{d}n}\right] = 0, \tag{22}$$

and the associated boundary conditions are $T(h/2) = T_t$ and $T(-h/2) = T_b$, where $\kappa(n)$ is the thermal conductivity in the thickness direction, while T_t and T_b denote the temperatures at the top and bottom surfaces of the FGM blade, respectively.

For these conditions, the solution of Eq. 22 is

$$T(n) = T_b\left[1 + \frac{\lambda}{\displaystyle\int_{-h/2}^{h/2}\frac{1}{\kappa(n)}\mathrm{d}n}\int_{-h/2}^{n}\frac{1}{\kappa(n)}\mathrm{d}n\right], \tag{23a}$$

where

$$\lambda = \frac{T_t - T_b}{T_b} \tag{23b}$$

constitutes a measure of the normalized temperature gradient across the blade wall thickness. Throughout the numerical simulations, $T_b = 300\,\mathrm{K}$ will be considered.

The thermal conductivity $\kappa(n)$ of the FGM is assumed to vary according to the law

$$\kappa(n) = (\kappa_c - \kappa_m)V_c + \kappa_m, \tag{24}$$

where that thermal conductivities κ_c and κ_m are considered to be temperature-independent.

The properties of the FGM are considered to be temperature-dependent, and to vary according to the law obtained from experiments. The temperature dependence is expressed in a generic form as

$$P(n) = P_0(P_{-1}/T + 1 + P_1T + P_2T^2 + P_3T^3), \tag{25}$$

where P_0, P_{-1}, P_1, P_2 and P_3 are the constants in the cubic fit of the specific temperature-dependent material property, where T (in Kelvin) is the environmental temperature, (see [4,11]).

As an alternative procedure, the Mori–Tanaka mean-field scheme can be applied to evaluate the local effective material properties (see [11]). Comparisons of the application of both Mori–Tanaka and of the simpler one, previously presented, will be supplied later in the paper.

4 The equations of motion, boundary conditions, and the governing system

The equations of motion and the associated boundary conditions, suitable for the described blade model built up of FGMs, are derived via Hamilton's principle. This can be formulated as

$$\int_{t_0}^{t_1}(\delta\mathcal{K}-\delta\mathcal{W}+\delta V)\mathrm{d}t=0;\ \ \delta w_0=\delta\phi=0 \text{ at } t=t_0,t_1, \tag{26}$$

where $\mathcal{K}$ and $\mathcal{W}$ denote the kinetic and strain energy, respectively, δV is the virtual work of external forces, t_0 and t_1 are two arbitrary instants of time, while δ is the variation operator.

Having in view that

$$\int_{t_0}^{t_1}\delta\mathcal{K}\mathrm{d}t=-\int_{t_0}^{t_1}\mathrm{d}t\int_{\tau}[\rho(a_x\delta u+a_y\delta v+a_z\delta w)]\mathrm{d}\tau, \tag{27}$$

where Hamilton's condition for $t=t_0,t_1$ was implied, using (15) and $\mathrm{d}\tau=\mathrm{d}\sigma\,\mathrm{d}z(=\mathrm{d}s\,\mathrm{d}n\,\mathrm{d}z)$, collecting the terms associated with the same variations $\delta\phi$ and δw_0, performing the integration by parts as to relieve $\delta\phi$ and δw_0 of any differentiation with respect to the z-variable, and recalling that the product of inertia with respect to the principal axes is zero, i.e., $\oint\eta\mathrm{d}s=0$, one obtains Eq. 27 in the form

$$\begin{aligned}\int_{t_0}^{t_1}\delta\mathcal{K}\mathrm{d}t\ =\ -\int_{t_0}^{t_1}\Bigg\{\int_0^L\Big[&b_1[\ddot{w}_0-(R_0+z+w_0)\Omega^2]\delta w_0\\&+\{I_p\ddot{\phi}+(I^0_{\zeta\zeta}-I^0_{\eta\eta})\Omega^2MN-[I_{ww}(\ddot{\phi}'-\Omega^2\phi')]'\}\delta\phi\Big]\mathrm{d}z+\Big[I_{ww}(\ddot{\phi}'-\Omega^2\phi')\delta\phi\Big]_0^L\Bigg\}\mathrm{d}t.\end{aligned} \tag{28}$$

The expression of the cross-sectional quantities is supplied in Table 1, where $(m_0,\ m_2)$ denote the reduced mass terms per unit beam length defined by

$$(m_0;m_2)=\int_{-h/2}^{h/2}[(\rho_c-\rho_m)V_c(1;n^2)+V_m(1;n^2)]\mathrm{d}n. \tag{29}$$

On the other hand, for the coupled twist–extension motion, $\delta\mathcal{W}$ is expressed as follows:

$$\delta\mathcal{W}\ =\ \frac{1}{2}\oint\int_0^L\left(N_{zz}\delta\varepsilon^{(0)}_{zz}+L_{zz}\delta\varepsilon^{(1)}_{zz}+N_{sz}\delta\gamma_{sz}\right)\mathrm{d}s\,\mathrm{d}z, \tag{30}$$

where $\varepsilon^{(0)}_{zz}$ and $\varepsilon^{(1)}_{zz}$ are provided by (13), while

$$\gamma_{sz}=\psi(s,z)\phi'(z), \tag{31}$$

Table 1 Cross-section quantities

Quantity	Definition
$I_p(\equiv I^0_{\zeta\zeta}+I^0_{\eta\eta})$	$m_0\oint(\eta^2+\zeta^2)\mathrm{d}s$
$\bar{I}_p$	I_p/m_0
I_{ps}	$\oint(\eta^2+\zeta^2)^2\mathrm{d}s$
$I^0_{\eta\eta}$	$m_0\oint\zeta^2\mathrm{d}s$
$I^0_{\zeta\zeta}$	$m_0\oint\eta^2\mathrm{d}s$
I_{ww}	$m_0\oint\bar{F}^2\mathrm{d}s+m_2\oint r_t^2\mathrm{d}s$
$\mathcal{B}$	$K_{11}[I_{ps}-\bar{I}_p^2/S]$
$S(z)$	$\oint\mathrm{d}s$

where $\psi(s)$ denotes the torsional function (see [4]).

In view of the previous equations, Eq. 30 reduces to

$$\delta\mathcal{W} = \int_0^L \left[T_z\delta w_0' - B_w\delta\phi'' + T_r\phi'\delta\phi' + M_z\delta\phi'\right]\mathrm{d}z, \tag{32}$$

where

$$T_z(z,t) = \oint N_{zz}\mathrm{d}s, \quad T_r(z,t) = \oint N_{zz}(\eta^2+\zeta^2)\mathrm{d}s, \quad B_w(z,t) = \oint[\bar{F}(s,z)N_{zz} - r_t(s,z)L_{zz}]\mathrm{d}s,$$

$$M_z(z,t) = \oint[N_{zz}(\eta^2+\zeta^2)\beta' + \psi(s,z)N_{sz}]\mathrm{d}s, \tag{33a, b, c, d}$$

denote the 1-D stress measures. The expressions of the 2-D stress resultants N_z, N_{sz} and stress couple L_{zz} intervening in (33) are given by

$$N_{zz} = K_{11}\varepsilon_{zz}^{(0)} + K_{14}\varepsilon_{zz}^{(1)} - \hat{N}_{zz}^T, \quad N_{sz} = K_{23}\phi', \quad L_{zz} = K_{41}\varepsilon_{zz}^{(0)} + K_{44}\varepsilon_{zz}^{(1)} - \hat{L}_{zz}^T, \tag{34a, b, c}$$

In (34), K_{ij} are 2-D stiffness quantities whose expressions are provided in the Appendix, while $\hat{N}_{zz}^T$ and $\hat{L}_{zz}^T$ are contributions brought on by the temperature field. Their expressions are

$$\hat{N}_{zz}^T = \left(1 - \frac{A_{12}}{A_{11}}\right)N_{zz}^T, \quad \hat{L}_{zz}^T = \left(L_{zz}^T - \frac{B_{12}}{A_{11}}N_{zz}^T\right) \tag{35}$$

where

$$(N_{zz}^T, L_{zz}^T) = \int_{-h/2}^{h/2}(Q_{11}+Q_{12})\hat{\alpha}\Delta T(1,n)\mathrm{d}n. \tag{36}$$

Carrying out integrations by parts in Eq. 32 so as to relieve the virtual displacements of any differentiation, one obtains

$$\int_{t_0}^{t_1}\int_0^L \delta\mathcal{W}\mathrm{d}z\,\mathrm{d}t = \int_{t_0}^{t_1}\left\{\int_0^L -\left[T_z'\delta w_0 + (B_\omega'' + (T_r\phi')' + M_z')\delta\phi\right]\mathrm{d}z + \left[T_z\delta w_0 - B_\omega\delta\phi' + (B_\omega' + T_r\phi' + M_z)\delta\phi\right]_0^L\right\}\mathrm{d}t. \tag{37}$$

Including in Hamilton's principle also the virtual work of external loads, (see [4]), collecting the terms associated with the same virtual displacements, and keeping in mind that the virtual displacements are independent and arbitrary within the spatial and time intervals $[0, L]$ and $[t_0, t_1]$, respectively, by setting their coefficients to zero, results in the equations of motion:

• *Equations of motion:*

$$\delta w_0 : T_z' - b_1\ddot{w}_0 + \underline{b_1\Omega^2(R_0+z+w_0)} + p_z = 0, \tag{38a}$$

$$\delta\phi : \underline{B_w''} + [T_r\phi']' + M_z' - I_p\ddot{\phi} + \underset{\sim\sim}{(I_{\eta\eta}^0 - I_{\zeta\zeta}^0)}\Omega^2 MN + \left[\underline{\underline{I_{ww}(\ddot{\phi}' - \Omega^2\phi')}}\right]' + m_z + \underline{m_w'} = 0, \tag{38b}$$

and in the related boundary conditions (BCs).

• For cantilevered blades these are: at $z = 0$:

$$\phi = \underline{\phi'} = w_0 = 0, \tag{39}$$

and at $z = L$:

$$T_z = h_1;\ \underline{B_w'} = h_w; \quad \text{and} \quad \underline{B_w'} + M_z + T_r\phi' + \underline{\underline{I_{ww}(\ddot{\phi}' - \Omega^2\phi')}} = h_\beta. \tag{40}$$

In (38), $p_z(\equiv p_z(z,t))$, $m_z(\equiv m_z(z,t))$ and $m_w(\equiv m_w(z,t))$ denote the distributed longitudinal external load, twist and warping moment, respectively, while the terms appearing in the right-hand side of BCs at $z = L$ are associated with the temperature field, their definition being as follows:

$$h_1 = \oint \hat{N}^T_{zz} \mathrm{d}s, \; h_w = \oint [\overline{F}(s)\hat{N}^T_{zz} - r_t(s)\hat{L}^T_{zz}]\mathrm{d}s,$$
and
$$h_\beta = \beta' \oint (\eta^2 + \zeta^2)\hat{N}^T_{zz}\mathrm{d}s. \tag{41}$$

It should be remarked that, due to the stipulated thickness-wise dependence of the temperature field, h_1, h_w and h_β are spanwise independent thermal terms and, as a result, these appear explicitly in the boundary conditions, at $z = L$, only, and not in the equations of motion.

Consistent with the three boundary conditions at each edge, the governing system should be of the sixth order. For small twist angles, implying $\sin\phi \Rightarrow \phi$ and $\cos\phi \rightarrow 1$, the tennis-racket term underscored in Eq. 38b by an undulated line becomes

$$(I^0_{\eta\eta} - I^0_{\zeta\zeta})\Omega^2 MN \rightarrow (I^0_{\eta\eta} - I^0_{\zeta\zeta})\Omega^2[\sin\beta\cos\beta + \phi\cos 2\beta]. \tag{42}$$

In the previous and the subsequent equations, the terms underscored by one and two superimposed dashed lines are associated with the warping restraint and warping inertia, respectively.

By virtue of Eqs. 33a,b, the second term in (38b) is expressed in terms of T_z as:

$$[T_r\phi']' = T_r'\phi' + T_r\phi'' = \frac{T_z'\bar{I}_p}{S}\phi' + \frac{T_z\bar{I}_p}{S}\phi''. \tag{43}$$

Now, Eq. 38b in conjunction with these last equations, becomes

$$\delta\phi: -[\underline{a_{66}}\underline{\phi''}]'' + \left(\underline{\frac{T_z\bar{I}_p}{S}\phi'}\right)' + [a_{71}w_0' + a_{77}\phi']' - I_p\ddot{\phi}$$
$$+ \underset{\sim\sim\sim\sim\sim\sim\sim\sim\sim\sim\sim\sim\sim\sim\sim\sim\sim\sim\sim}{(I^0_{\eta\eta} - I^0_{\zeta\zeta})\Omega^2[\sin\beta\cos\beta + \phi\cos 2\beta]} + [\underline{\underline{I_{ww}}}(\underline{\underline{\ddot{\phi}'}} - \Omega^2\underline{\underline{\phi'}})]' + m_z + \underline{m_w'} = 0, \tag{44}$$

whereas (38a) remains unchanged. As concerns the 1-D stiffness quantities a_{66}, a_{77} and a_{71} their expressions are provided in the Appendix.

In order to reduce the governing equations to a single equation, w_0 should be exactly eliminated in (38). Paralleling the procedure followed in [4,5], the governing equations reduce to

$$-[\underline{a_{66}}\underline{\phi''}]'' + \left(\underline{\frac{T_z\bar{I}_p}{S}\phi'}\right)' + (\mathcal{B}\beta'^2\phi')' - I_p\ddot{\phi}$$
$$+ \underset{\sim\sim\sim\sim\sim\sim\sim\sim\sim\sim}{(I^0_{\eta\eta} - I^0_{\zeta\zeta})\Omega^2\phi\cos 2\beta} + [\underline{\underline{I_{ww}}}(\underline{\underline{\ddot{\phi}'}} - \Omega^2\underline{\underline{\phi'}})]' + m_z + \underline{m_w'} = -\left(\frac{a_{71}T_z}{K_{11}S}\right)', \tag{45}$$

and the boundary conditions to
At $z = 0$:

$$\phi = \underline{\phi'} = 0, \tag{46}$$

and at $z = L$:

$$\underline{a_{66}}\underline{\phi''} = -h_w, \quad -(\underline{a_{66}}\underline{\phi''})' + \underline{\frac{T_z\bar{I}_p}{S}}\phi' + \mathcal{B}\beta'^2\phi' + \underline{\underline{I_{ww}}}(\underline{\underline{\ddot{\phi}'}} - \Omega^2\underline{\underline{\phi'}}) + \frac{a_{71}}{K_{11}S}T_z = h_\beta. \tag{47}$$

As concerns the expression of T_z, the neglect of the axial inertia and load terms in Eq. 38a, followed by its integration with respect to z, and in conjunction with the related BC at $z = L$, yields

$$T_z(z) = \int_z^L b_1\Omega^2(R_0 + z)\mathrm{d}z + h_1. \tag{48}$$

As it clearly appears, the terms in (45) and the BCS (47b) underscored by the dotted line are due to the tension–twist coupling, in which also the temperature is involved. However, by virtue of (48), T_z in (47b) reduces to h_1.

As a result of (48), the governing equation (45) and the boundary conditions (46) and (47) become expressed in terms of the unknown function $\phi(z, t)$ only.

These equations govern the motion of pretwisted rotating thin-walled beams of non-uniform cross-section, built up of FGMs, exposed to a steady-state temperature field, and featuring the twist–extension elastic coupling.

For the free-warping case the terms underscored by a dashed line become immaterial and, as a result, the governing equation becomes of the second order. This implies that a single boundary condition at each edge is required.

Until this point, in the governing equations no specific variation of the pretwist angle β along the beam span has been prescribed. In the numerical simulations, a linear variation, implying $\beta(z) = \beta_0 z/L$, where β_0 is the pretwist at the beam free end will be considered.

5 The eigenvalue problem

Due to the complicated natural boundary conditions at the blade tip which, in addition, are non-homogeneous, the Extended Galerkin Method is used [2,4,12]. Within this method, admissible trial functions that satisfy only the geometric boundary conditions are employed. In spite of this, the residual terms that are the result of the non-fulfillment of the governing equation and of natural boundary conditions are minimized in Galerkin's sense, this yielding a high accuracy of the solution. To this end, one considers the solution in the form

$$\phi(z, t) = \mathbf{F}^T(z)\mathbf{q}_\phi(t), \;\; w_0(z, t) = \mathbf{W}^T(z)\mathbf{q}_w(t), \tag{49}$$

where $\mathbf{F}$, $\mathbf{W}$ and $\mathbf{q}_\phi$, $\mathbf{q}_w$ are N-dimensional column vectors of trial functions and generalized coordinates, respectively, while superscript T denotes the transpose operation. Replacement of (49) in the variational integral (26), after performing all the indicated operations and the required integrations, the discretized system results as

$$\mathbf{M}\ddot{\mathbf{q}}(t) + \mathbf{K}\mathbf{q}(t) = \mathbf{Q}(t). \tag{50}$$

Here $\mathbf{q} = \left\{\mathbf{q}_\phi^T, \; \mathbf{q}_w^T\right\}^T$ is the $2N \times 1$ vector of generalized coordinates, $\mathbf{M}|_{2N\times 2N}$ and $\mathbf{K}|_{2N\times 2N}$ are the symmetric mass and stiffness matrices, respectively, while $\mathbf{Q}$ is the load vector. Using the method presented in [4], one may express Eq. 50 in state-space form. In this sense, defining the $4N \times 1$ state vector $\mathbf{X} = \left\{\mathbf{q}^T, \dot{\mathbf{q}}^T\right\}^T$ and adjoining the identity $\dot{\mathbf{q}} = \dot{\mathbf{q}}$, one obtains Eq. 50 in the form

$$\dot{\mathbf{X}}(t) = \mathbf{A}\mathbf{X}(t), \tag{51}$$

where the $4N \times 4N$ state matrix $\mathbf{A}$ is

$$\mathbf{A} = \begin{bmatrix} \mathbf{0} & \mathbf{I} \\ -\mathbf{M}^{-1}\,\mathbf{K} & \mathbf{0} \end{bmatrix}, \tag{52}$$

while $\mathbf{I}$ and $\mathbf{0}$ are the identity and the zero matrices, respectively. Expressing $\mathbf{X}(t)$ in (51) as

$$\mathbf{X}(t) = \mathbf{Z}\exp(\Lambda t), \tag{53}$$

a standard eigenvalue problem is obtained

$$(\mathbf{Z} - \Lambda\mathbf{I})\mathbf{X} = 0, \tag{54}$$

which can be solved for the eigenvalues Λ_r and the eigenvector $\mathbf{X}$. In the present case, $\Lambda_r = \pm \mathrm{i}\omega_r$, that implies harmonic oscillations.

Table 2 Comparison of percentage frequency rise ratio for a non-rotating blade, featuring selected pre-twist angles

Mode	$\beta_0 = 15$ deg.		$\beta_0 = 30$ deg.		$\beta_0 = 45$ deg.		$\beta_0 = 60$ deg.	
No.	Ref. [13]	Present	Ref. [13]	Present	Ref. [13]	Present	Ref. [13]	Present
$b/c = 0.05$								
1	11.895	11.888	41.19	41.181	79.042	79.031	120.879	120.905
2	10.338	10.333	36.082	36.080	69.775	69.795	107.377	107.485
3	8.000	8.003	28.544	28.557	56.163	56.208	87.540	87.659
$b/c = 0.20$								
1	0.708	0.788	3.032	3.121	6.781	6.879	11.978	11.900
2	0.680	0.686	2.697	2.685	5.953	5.973	10.311	10.354
3	0.52	0.527	2.058	2.086	4.567	4.623	7.954	8.054

6 Validations of the solution methodology and of the FGM model

The validations will encompass:

(i) The accuracy of the adopted solution methodology, and
(ii) The accuracy of predictions based on the simple rule of mixtures (R. M) as compared with those by the Mori–Tanaka (M-T) homogenization scheme.

For point (i) above, the comparisons will involve the case of a purely metallic non-rotating pre-twisted blade. In this sense, comparisons of the percentage rise involving the frequency ratio of pre-twisted blade with the counterpart value of the untwisted blade are supplied in Table 2 for the first three mode numbers.

The percentage rise is defined as: $[(\omega_n)_{\beta_0} - (\omega_n)_{\beta_0=0}] \times 100/(\omega_n)_{\beta_0=0}$ and the comparisons have been done with predictions of [13] for a blade characterized by length ratio $L/c = 2$.

The results of these comparisons reveal an excellent agreement. The second set of validations involve non-rotating ($\Omega = 0$) and un-twisted ($\beta_0 = 0$) FGM blades whose phases vary from ceramic to metal. The first three dimensionless eigenfrequencies $\overline{\omega}_i = \omega_i/\hat{\omega}_1$ where the normalizing frequency $\hat{\omega}_1 = 1187$ rad/s corresponds to $\lambda = 0,\ \Omega = 0,\ \beta_0 = 0$ and to the fully metallic blade of cross-section ratio $c/b = 1$, are supplied in Table 3. These have been obtained for two values of the temperature gradient λ and for selected values of the volume-fraction parameter K, ranging from $K = 0$ (full ceramic) to $K = 50$ (full metal) evaluated on the basis of the R. M. and the M–T schemes. The supplied results reveal an excellent agreement between the two predictions.

7 Results and discussion

Although the obtained equations are valid for a beam of arbitrary closed cross-section, for the sake of illustration, the case of a rotating beam modeled as an FGM box-beam, (see Fig. 1), characterized, unless otherwise specified, by $\bar{R} = R_0/L = 0.1;\ L/c = 8;\ c = 0.254$ m; $b = 50.8 \times 10^{-3}$ m implying a cross-section ratio $\mathcal{R}(\equiv c/b) = 5$, and $h = 10.16 \times 10^{-3}$ m, was considered. In addition, the two constituents of the graded beam are from silicon nitride (SN) and stainless steel (SS). The constants P_i as involved in Eq. 25, associated with each of these constituent phases can be found in [4,12], and will not be supplied here.

Figures 2a–c display in succession for a pre-twisted ($\beta_0 = 30$deg) and non-rotating blade, the variation of the first three eigenfrequencies as a function of the increase of the upper temperature, and for selected values of the volume-fraction exponent ranging from that corresponding to full ceramic, ($K = 0$), until full metal ($K = 50$).

The results reveal that the full ceramic blade experiences the largest eigenfrequencies, and the decay, as a result of the temperature increase, is more accentuated for the fully metallic blade.

Table 3 Comparison of the natural frequencies based on Mori–Tanaka (M–T) and the simple rule of mixtures (R. M), for selected values of the volume-fraction exponent and two values of the temperature gradient λ, ($\Omega = 0,\ \beta = 0$)

Volume fraction exponent	Dimensionless eigenfrequency $\overline{\omega}_i$	$\lambda = 0$		$\lambda = 3$	
		R. M	M–T	R. M	M–T
$K = 0$ (ceramic)	$i = 1$	2.384	2.384	2.292	2.292
	$i = 2$	7.165	7.165	6.886	6.886
	$i = 3$	11.98	11.98	11.49	11.49
$K = 0.2$	$i = 1$	1.943	1.932	1.858	1.846
	$i = 2$	5.826	5.794	5.578	5.533
	$i = 3$	9.729	9.675	9.313	9.241
$K = 0.5$	$i = 1$	1.647	1.634	1.569	1.548
	$i = 2$	4.945	4.905	4.708	4.053
	$i = 3$	8.255	8.189	7.861	7.76
$K = 50$ (metal)	$i = 1$	1.000	1.000	0.882	0.882
	$i = 2$	3.008	3.008	2.647	2.647
	$i = 3$	5.019	5.019	4.420	4.420

Figures 3a–c depict the influence of the dimensionless rotational speed $\overline{\Omega}(= \Omega/\hat{\omega}_1)$ coupled with that of the volume-fraction exponent K on the first three dimensionless eigenfrequencies. The results reveal that the centrifugal effects play a stronger beneficial role on metallic blades than on those featuring an increase of the ceramic phase.

This is due to the fact that the full ceramic blades are stiffer than their metallic counterparts, and as a result, are less sensitive to the centrifugal stiffening effect. However, for any $\overline{\Omega}$, the decrease of K from $K = 50$ to $K = 0$, i.e., an increase of the ceramic phase yields an increase of the natural eigenfrequencies.

However, the increase of $\overline{\Omega}$ yields an alleviation of the detrimental role of the temperature-gradient increase, a trend that becomes stronger with the increase of λ.

This is attributed to the fact that the increase of λ, together with the thermal degradation, yields a decay of the stiffness characteristics of the blade, and due to this increased flexibility, the blade becomes more sensitive to the stiffening effect provided by the increase of $\overline{\Omega}$.

In Fig. 4a–c, the influence of $\overline{\Omega}$ coupled with that of the normalized temperature gradient across the blade thickness on the first three dimensionless eigenfrequencies is presented for the case of a FGM blade whose ceramic–metal constituents are mixed. The results reveal that, in general, an increase of λ plays a detrimental role on eigenfrequencies.

Figures 5a–c present the influence of the pre-twist coupled with that of the volume-fraction exponent on the first three dimensionless eigenfrequencies for a non-rotating blade. The results reveal that, in general, an increase of the ceramic phase materialized by an decrease of K, yields an increase of $\overline{\omega}_i$ for any value of β_0. However, it appears that the increase of $\overline{\omega}_i$ with the increase of β_0 is stronger for the blades madeup of graded ceramic-metal constituents than for the fully metallic ones.

Figure 6a–c depict the three normalized mode shapes in twist of the non-rotating/rotating blade made up of full metal (Fig. 6a), from a mixture of ceramic–metal, (Fig. 6b), and of full ceramic (Fig. 6c). As it can be seen, the increase of $\overline{\Omega}$ yields, in general, a shift of nodal points toward the blade tip.

However, with the increase of the proportions of the ceramic phase, there is a dramatic decay of this trend, and for the fully ceramic blade, the implications of $\overline{\Omega}$ on the first three eigenvalues become totally marginal. This trend is attributed to the decay of blade's flexibility, once the proportions of the ceramic phase increase in the blade composition.

Finally, the obtained results not shown here reveal that, while the elastic warping yields an increase of the eigenfrequencies for any K and for the relatively small L/c ratio blades, the influence of the inertial warping is marginal.

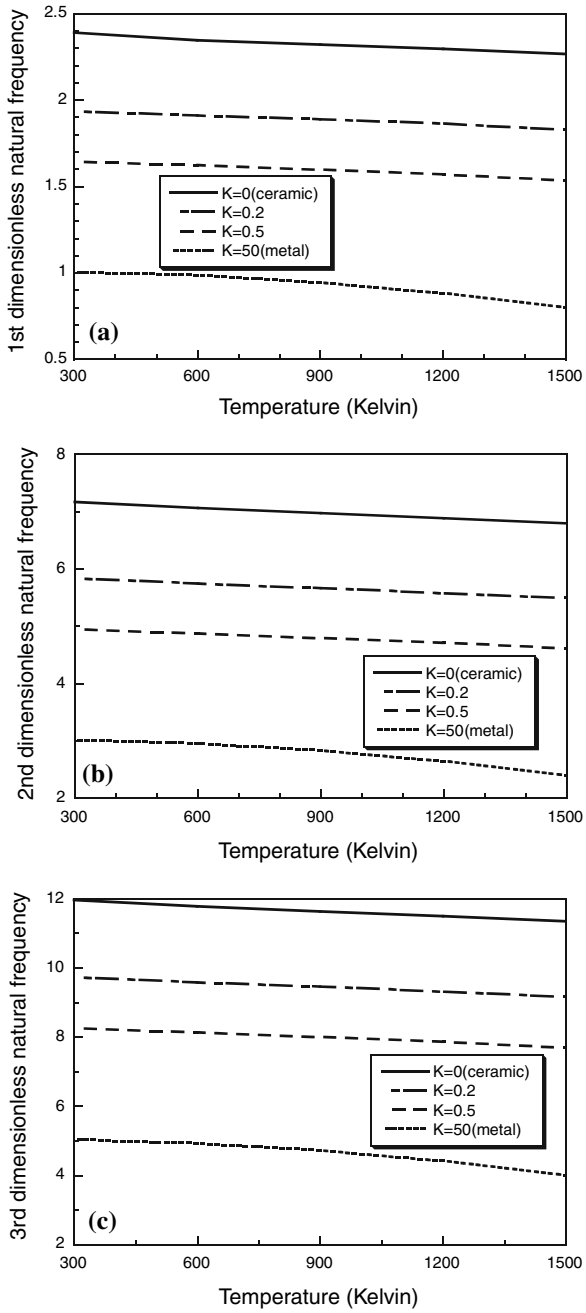

Fig. 2 Effects of the upper temperature rise and of the volume-fraction parameter K on the first three dimensionless eigenfrequencies $\overline{\omega}_i\,(\beta_0 = 30\ \text{deg.},\ \Omega = 0)$. (**a**) $\overline{\omega}_1$; (**b**) $\overline{\omega}_2$; (**c**) $\overline{\omega}_3$

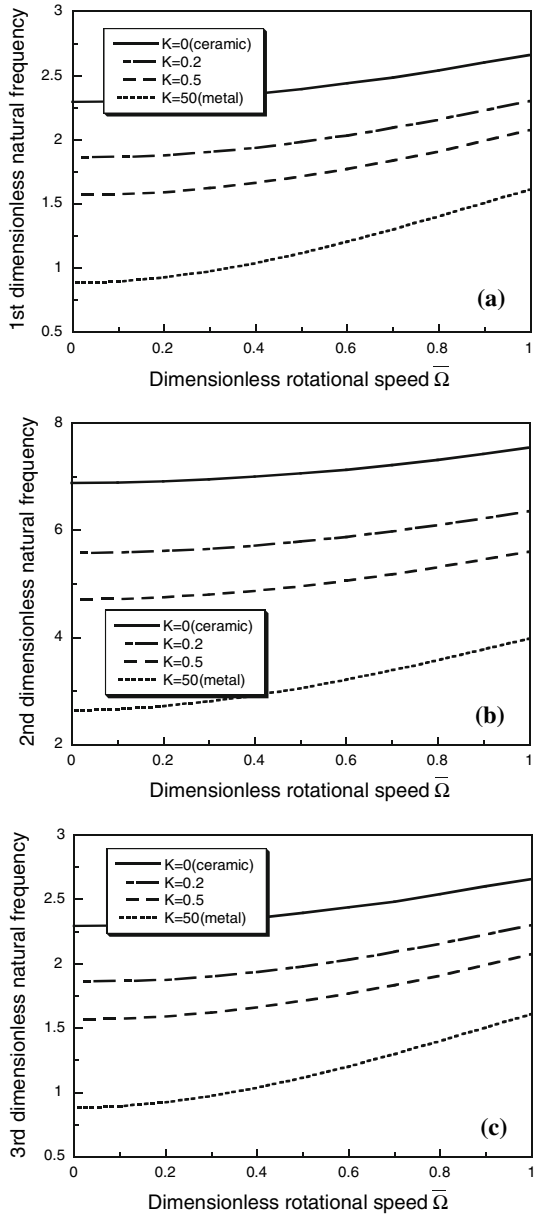

Fig. 3 The influence of the variation of the dimensionless rotational speed and of volume-fraction parameter K on the first three dimensionles eigenfrequency $\overline{\omega}_i$ $(\lambda = 3,\ \beta_0 = 30\,\text{deg.})$ (**a**) $\overline{\omega}_1$; (**b**) $\overline{\omega}_2$; (**c**) $\overline{\omega}_3$

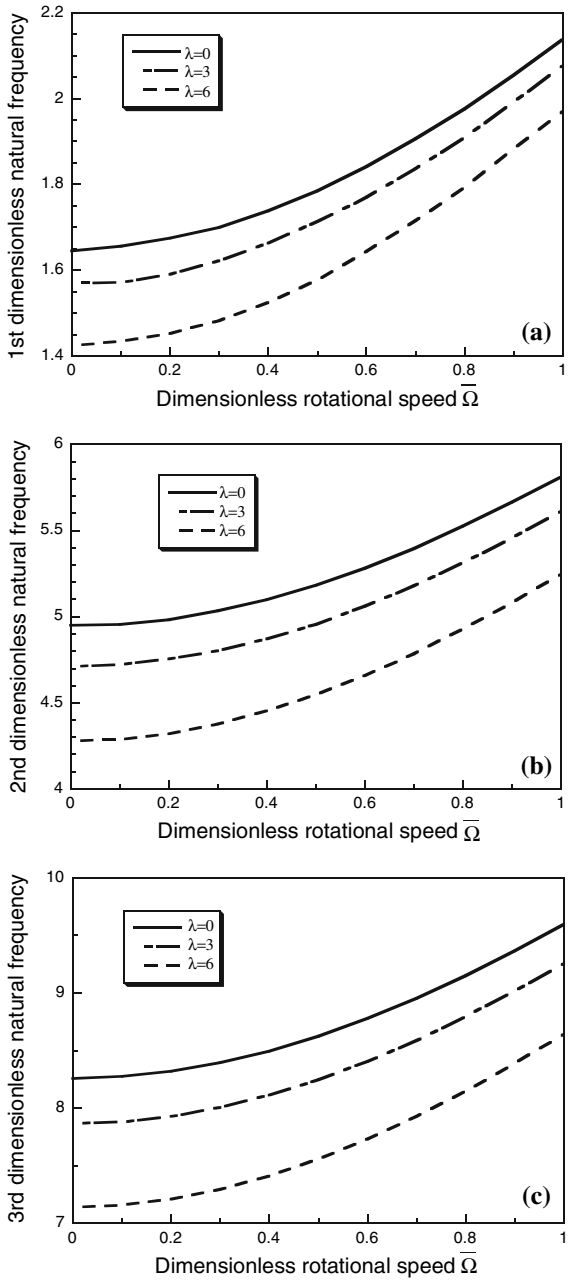

Fig. 4 Effects of the variation of the dimensionless rotational speed and of the normalized temperature gradient λ on the first three dimensionless eigenfrequencies $\overline{\omega}_i$, ($K = 0.5, \beta_0 = 30$ deg.) (**a**) $\overline{\omega}_1$; (**b**) $\overline{\omega}_2$; (**c**) $\overline{\omega}_3$

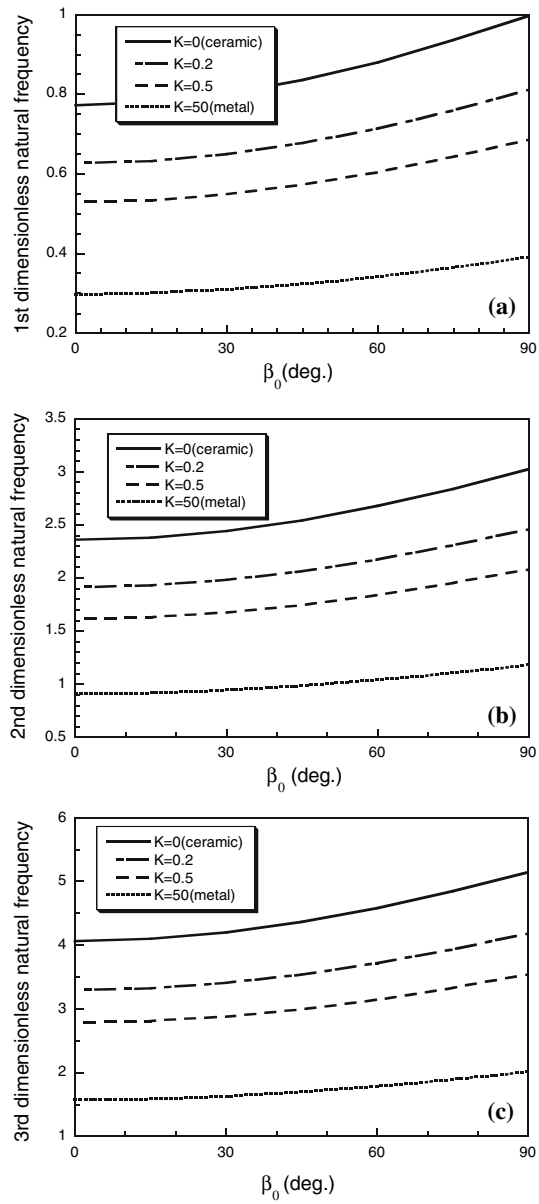

Fig. 5 Implications of the pre-twist angle and of the volume fraction parameter on the first three dimensionless eigenfrequencies $\overline{\omega}_i$ of non-rotating blade ($\lambda = 3,\ \Omega = 0,\ L$ = fixed, $L/c = 5, \overline{R} = 0.05$; (**a**) $\overline{\omega}_1$; (**b**) $\overline{\omega}_2$; (**c**) $\overline{\omega}_3$

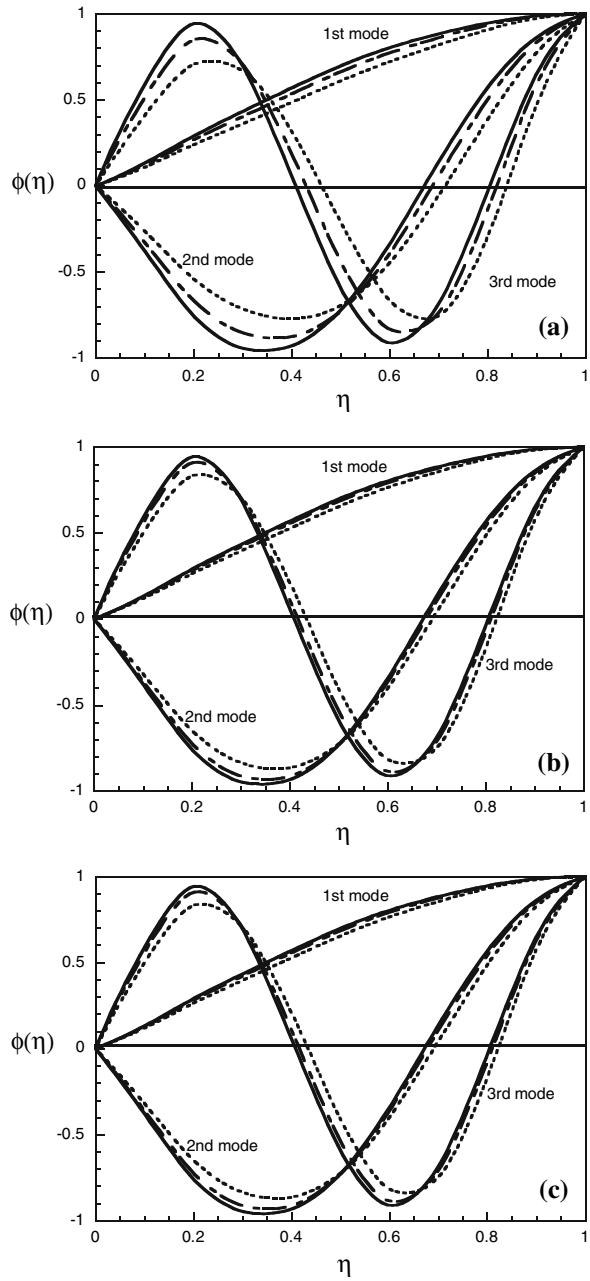

Fig. 6 Variation of torsional mode shapes for selected rotational speeds ($\lambda = 3$, β_0=0, _____ $\overline{\Omega} =$ 0 ——–—– $\overline{\Omega} =$ 0.5 ..... $\overline{\Omega} = 1.0$, and for three values of the volume-fraction exponent, K: (**a**) $K = 50$, (**b**) $K = 0.5$, (**c**) $K = 0$

As concerns the tennis-racket term that depends on both the pre-twist and the rotational speed, the results in [4,5,7,8] reveal that it plays a softening role, in the sense of a decrease of the torsional eigenfrequencies. However, as the results reveal, the increase of the ceramic phase in the blade composition compensates this decrease. In contrast to it, the tension–torsion coupling terms materialized by the second term in (45) plays a beneficial role, in the sense of an increase of the torsional frequency with the increase of $\overline{\Omega}$, and this, for any K.

8 Conclusions

A study devoted to the modeling and vibrational behavior of thin-walled FGM rotating blades featuring the extension–twist elastic coupling and exposed to a temperature field has been presented. In this context, the implications on the eigenfrequencies and mode shapes of the proportions of the two phases in the constitution of the FGM, that is, ceramic and metal, measured in terms of the volume-fraction parameter K, have been put into evidence. The thermal degradation of the material characteristics has been included in the structural model, and its effects, considered in conjunction with the temperature gradient, the pre-twist, and the rotational speed, have been assessed. It is believed that the structural model and the reported results will play a useful role in the design of advanced rotor blades made up of FGMs and exposed to high-temperature gradients.

Appendix: Some coefficients

Expressions of the modified local stiffness quantities $K_{ij}(\equiv K_{ji})$.

$$K_{11} = A_{22} - \frac{A_{12}^2}{A_{11}};\ K_{14} = B_{22} - \frac{A_{12}B_{12}}{A_{11}},\quad K_{22} = A_{66} - \frac{A_{16}^2}{A_{11}};\ K_{23} = 2K_{22}\frac{A_c(z)}{S(z)},\quad K_{44} = D_{22} - \frac{B_{12}^2}{A_{11}},$$

A_{ij}, B_{ij} and D_{ij} being the standard local stretching, bending–stretching and bending-stiffness quantities, respectively.

Expressions of the global stiffness quantities $a_{ij}(\equiv a_{ji})$

$$a_{11} = \oint K_{11}\mathrm{d}s,\quad a_{71} = K_{11}\beta'\overline{I}_p,\quad a_{66} = \oint [K_{11}\overline{F}^2 - K_{14}\overline{F}r_t]\mathrm{d}s,\quad a_{77} = 2\oint \frac{A_c(z)}{S_(z)}K_{22}\mathrm{d}s + K_{11}I_{ps}(\beta')^2,$$

where A_c denotes the area of the blade cross-section.

References

1. Birman V, Byrd LW (in press) Modeling and analysis of functionally graded materials and structures. Appl Mech Rev
2. Librescu L, Oh S-Y, Song O (2005) Thin-walled beams made of functionally graded materials and operating in a high temperature environment: vibration and stability. J Thermal Stresses 28:649–712
3. Oh SY, Librescu L, Song O (2003) Thermoelastic modeling and vibration of functionally graded thin-walled rotating blades. AIAA J 41:2051–2060
4. Librescu L, Song O (2005) Thin-walled composite beams: theory and application. Springer 600 pp.
5. Oh S-Y, Librescu L, Song O (2005) Modeling and vibration of composite thin-walled rotating blades featuring extension-twist elastic coupling. The Aeronautical J 109:233–246
6. Houbolt JC, Brooks GW (1958) Differential equations of motion for combined flapwise bending, chordwise bending, and torsion of twisted nonuniform rotating blades. NASA TR 1364
7. Kaza KB, Kielb RE (1984) Effects of warping and pretwist on torsional vibration of rotating beams. ASME J Appl Mech 51:913–920
8. McGee OG (1992) Influence of warping-pretwist coupling on the torsional vibration of centrifugally-stressed cantilevers, with thin-walled open beams. Comput Struct 42:175–195
9. Washizu K (1964) Some considerations on a naturally curved and twisted slender beam. J Math Phys 43:111–116
10. Bauchau OA, Hong CH (1989) Large displacement analysis of naturally curved and twisted composite beams. AIAA J 25:1469–1475
11. Reddy JN, Chin CD (1998) Thermomechanical analysis of functionally graded cylinders and plates. J Thermal Stresses 21:593–626
12. Librescu L, Oh S-Y, Song O (2004) Spinning thin-walled beams mode of functionally graded materials: Modeling, vibration and instability. Eur J Mech A/Solids 23:499–515
13. Subrahmanyam KB, Kaza KRV (1985) Finite difference analysis of torsionally vibrations of pretwisted, rotating, cantilever beams with effects of warping. J Sound Vibration 99:213–224